Journal of Applied Mechanics and Technical Physics, Vol. 50, No. 3, pp. 532–539, 2009

CRACK PATH KINKING UNDER GENERALIZED STRESS STATE

A. G. Demeshkin and V. M. Kornev

UDC 539.3

Results of experimental investigations of three-point asymmetric bending applied to beams made of materials with substantially different structural, strength, and strain characteristics are presented. The effect of different types of fracture on the formation of crack kinks under a generalized stress state is revealed. Strength curves of the Coulomb–Mohr type are obtained for Plexiglas and fine-grained concrete, which are characterized by the quasi-brittle and brittle types of fracture, respectively. Dependences of the kink angles of the crack paths on the stress state in the case of three-point bending are described for these materials.

Key words: *brittle and viscous fracture, crack branching and kinking, critical stress-intensity factor.*

Introduction. There are few papers where the effect of material characteristics of crack kinking and branching is studied (see, e.g., [1–3]). The material characteristics are usually taken to mean both the original material structure (before the material is subjected to inelastic deformation) and the transformed material structure (after inelastic deformation).

1. Crack Branching in Real Materials. To obtain preliminary estimates of growth and branching of crack-like defects in real materials under conditions of the generalized stress state, three-point asymmetric bending experiments were performed with beams made of materials with substantially different structural, strength, and strain characteristics: spheroplastic, Plexiglas, D16T aluminum alloy, and St. 3 steel. A 1.5-mm wide cut of length l (in millimeters) simulating a crack was made in each beam. The loading scheme for the specimens, with the point force P applied at the center and the compressive stresses $\sigma < 0$ applied to the specimen flanks, is shown in Fig. 1. The length of the specimens between the piers is $L = 100$ mm, the length of the edge crack-cut is $l = 7.5$ mm for beams made of spheroplastic, Plexiglas, and D16T aluminum alloy and $l = 6.8$ mm for steel specimens, the distance between the applied point force and the crack is $s = 30$ mm, the height is $b = 20$ mm for beams made of spheroplastic, Plexiglas, and D16T aluminum alloy and $b = 17$ mm for steel specimens, the thickness of all specimens is $t \approx 10$ mm, and the kink angle of the crack path is α. The rigid, strength, and strain characteristics of spheroplastic, Plexiglas, D16T aluminum alloy, and St. 3 steel obtained by the authors of the present paper in preliminary experiments are summarized in Table 1; the characteristics of the D16T aluminum alloy and St. 3 steel agree with available reference data.

Spheroplastic is a typical brittle material, Plexiglas is a quasi-brittle material, the D16T aluminum alloy occupies an intermediate position between the quasi-brittle and quasi-viscous materials, St. 3 steel is a quasi-viscous material, and modified St. 3 steel, judging by the character of its fracture, is a quasi-brittle material (for the chosen scheme of fracture).

Three-point bending experiments were performed with specimens made of the above-indicated materials and modified St. 3 steel. The specimen was made of modified St. 3 steel in the following manner: a large specimen made of St. 3 steel in the original state without any damages was subjected to tension; the strain reached 22%; after that,

Lavrent'ev Institute of Hydrodynamics, Siberian Division, Russian Academy of Sciences, Novosibirsk 630090; kornev@hydro.nsc.ru. Translated from Prikladnaya Mekhanika i Tekhnicheskaya Fizika, Vol. 50, No. 3, pp. 205–213, May–June, 2009. Original article submitted January 11, 2008; revision submitted May 5, 2008.

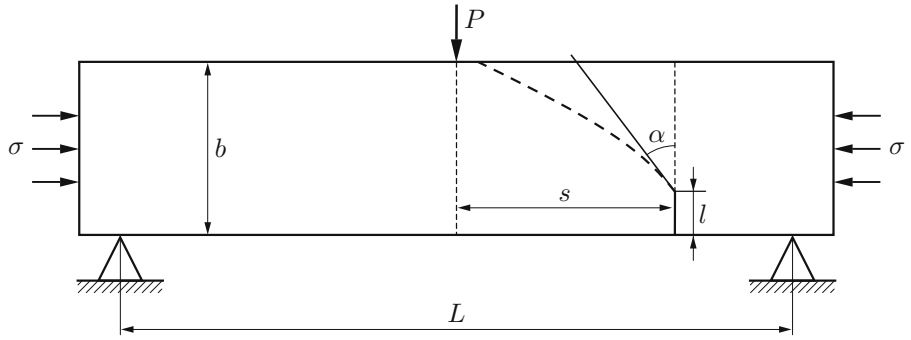

Fig. 1. Loading scheme: the solid curve is the tangent, and the dashed curve is the crack path.

TABLE 1

Characteristics of Specimen Materials

Material	E, MPa	σ_{02}, MPa	σ^*, MPa	ν	ε^*, %
Spheroplastic	2400	18–20	18–20	0.32	0.8–1.0
Plexiglas	3000	20–25	40–45	0.35	2.5–3.0
D16T alloy	$7 \cdot 10^4$	400–450	610	0.34	10–12
St. 3 steel	$20 \cdot 10^4$	220	400–450	0.28	≈25

Note. The following notation is used for material characteristics: Young's modulus E, limit of elasticity σ_{02}, limiting stresses at fracture σ^*, Poisson's ratio ν, and relative limiting elongation at which fracture occurs ε^*.

a beam was manufactured from this specimen, the beam axis being coincident with the tension direction; finally, a cut simulating the crack was made in the beam.

Figure 2 shows the photographs of five specimens ($j = 1, 2, \ldots, 5$) fractured in accordance with the loading scheme proposed (see Fig. 1). It is seen that the spheroplastic and Plexiglas specimens broke into fragments after the test, while the specimens made of the D16T aluminum alloy, St. 3 steel, and modified St. 3 steel remained relatively safe. Crack-like defects in specimens made of these materials extended by means of formation of kinked cracks from the tips of these defects under asymmetric three-point bending, propagation of the kinked cracks being substantially dependent on the material characteristics. Under inelastic deformation, St. 3 steel after modification transformed from a quasi-viscous state to a quasi-brittle state, i.e., St. 3 steel was embrittled after significant inelastic deformation [4]. It should be noted that the fracture behavior of specimens made of different materials is also different:

1) The Plexiglas specimen demonstrates quasi-brittle behavior; the specimen made of the D16T aluminum alloy is characterized by an intermediate fracture type between the quasi-brittle and quasi-viscous types; the curvatures $\varkappa_j$ ($j = 4, 3$) of the kinks from the tips of the crack-like defects have different signs: if $\varkappa_4 < 0$, then $\varkappa_3 > 0$;

2) The specimen made of St. 3 steel demonstrates quasi-viscous behavior; the specimen made of modified St. 3 steel is characterized by quasi-brittle fracture; the curvature of the kinked curve from the tip of the crack-like defect differs from zero ($\varkappa_2 \neq 0$) for St. 3 steel and is close to zero ($\varkappa_1 \approx 0$) for modified St. 3 steel, and the angle between the kinked curves is close to $\pi/2$;

3) Specimen Nos. 3–5, which demonstrate brittle, quasi-brittle, and intermediate between quasi-brittle and quasi-viscous fracture, differ from specimen Nos. 1 and 2 by significant contraction that appears in the pre-fracture zone of the two latter specimens, though their fracture can be classified as quasi-viscous and quasi-brittle.

The fracture criteria proposed in [1, 2] are in qualitative agreement with the results of full-scale experiments conducted with macrospecimens, where Mode I fracture is observed. For brittle and quasi-brittle materials, it is reasonable to use the Erdogan–Sih hypothesis [5].

2. Crack Kinking Under Three-Point Bending. Let us consider crack branching and crack path kinking under a controlled combined action of tensile and shear stresses on quasi-brittle and brittle materials in

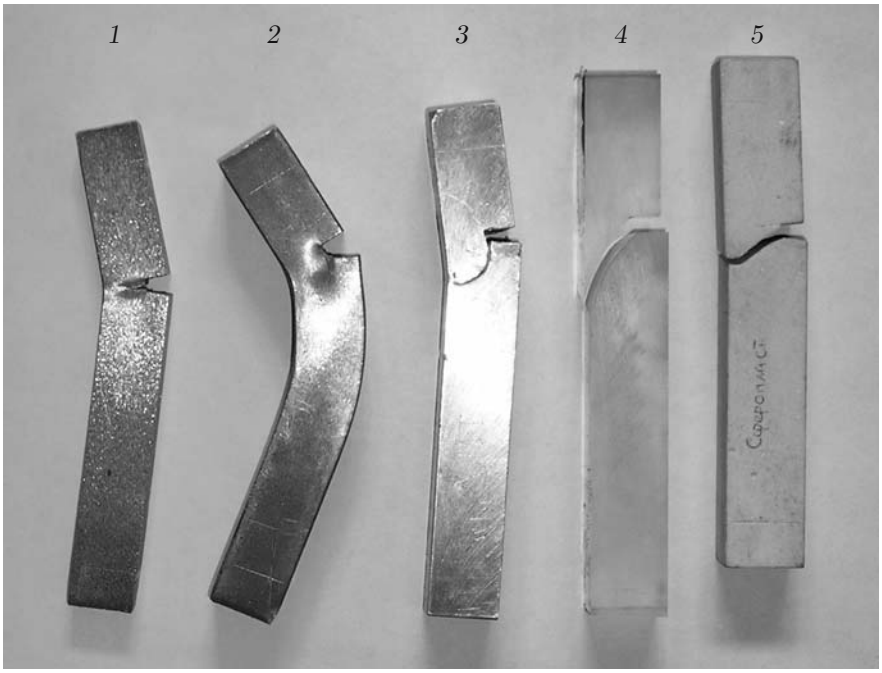

Fig. 2. Photographs of five fractured specimens made of modified St. 3 steel (1), St. 3 steel (2), D16T aluminum alloy (3), Plexiglas (4), and spheroplastic (5).

more detail. Fault branching and initiation of new faults during earthquakes were studied in [6]. In terms of the fracture type, rocks can be classified as brittle or quasi-brittle materials. Fracture of rocks under conditions of the generalized stress state depends on the type of loading and rock structure [7, 8]. Polymethylmethacrylate (Plexiglas) and fine-grained concrete refer to quasi-brittle and brittle materials. Experiments involved three-point bending applied to beams with additional compressive loading of the flanks. Strength curves of the Coulomb–Mohr type [8] were constructed for these materials, and the angles of crack branching [kink angles of the crack path α (see Fig. 1)] under controlled loading with variation of the parameter s were determined. Two cases were considered: $\sigma = 0$ and $\sigma \neq 0$.

2.1. *Experiments with Polymethylmethacrylate* (*Plexiglas*) *Specimens.* First, we construct a strength curve of the Coulomb–Mohr type for Plexiglas. The specimens were cut out of a Plexiglas plate 25 mm thick. At the first stage, we determined the tensile strength (48 MPa) and the compressive strength of a cube made of this material (-124 MPa). The experimentally obtained dependence of the normal stress on the specimen strain $\sigma(\varepsilon)$ is presented in Fig. 3 and in Table 2. Note that the modulus of elasticity under tension $E = 2600$ MPa in this case is slightly different from the value of this parameter for specimens made of a Plexiglas sheet (see Sec. 1).

To construct the strength curve of the Coulomb–Mohr type in the plane (σ, τ), we tested 10×10-mm specimens 25 mm long under shear loading (σ and τ are the normal and shear stresses). The shear load was applied to a 10×10-mm cross section between two piers located at a distance of 10 mm from each other. It should be noted that the specimen subjected to pure shear loading demonstrated brittle fracture and became fragmented, whereas the specimen compressed normal to its flanks exhibited plastic deformation without fragmentation (Fig. 4). The experimental data are summarized in Table 3, and Fig. 5 shows the strength curve of the Coulomb–Mohr type, which is plotted through the experimental points.

Further we consider the tests with three-point bending applied to the Plexiglas beam with a crack. In testing beams with a prescribed length of the edge crack l, we determined the kink angle of the crack path α as a function of the distance s from the center of specimen bending (the width of the cut simulating the crack was 1 mm). The specimen sizes were chosen to fit the Russian Standard (GOST) [9]: $L = 100$ mm, $b = 25$ mm, $l = 11.3$ mm, and $t = 12.5$ mm. The dependence $\alpha(s)$ was determined for two types of loading: $\sigma = 0$ and $\sigma \neq 0$ (see Fig. 1). Preliminary compression of the beam applied normal to the flanks corresponded to the value $\sigma = -1.25$ MPa. The

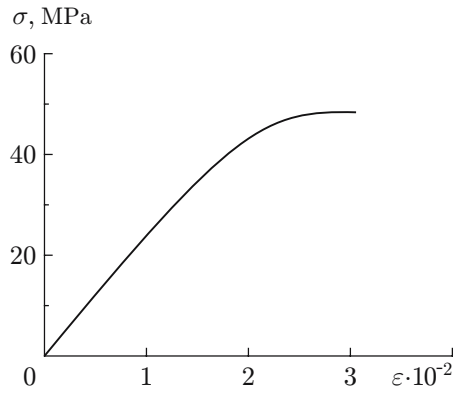

Fig. 3. Dependence $\sigma(\varepsilon)$ for the Plexiglas specimen under tension.

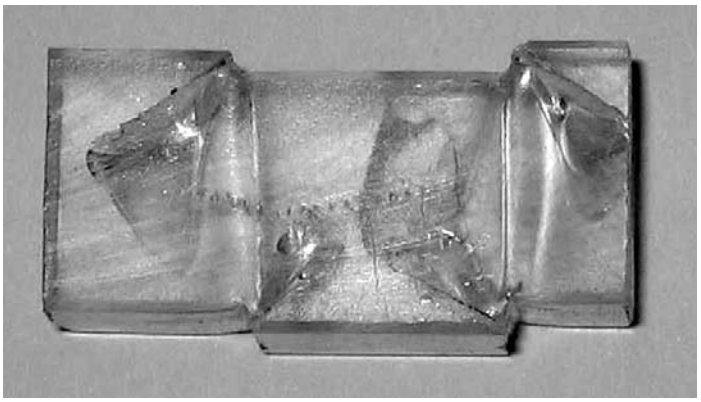

Fig. 4. Photograph of the fractured Plexiglas specimen in the experiment under shear loading with compression.

angle α is the angle between the tangent to the crack path kink at the crack tip and the original direction of the crack. The results of tests with three-point bending of the cracked Plexiglas beam are summarized in Table 4.

At least three beams were tested for each type of loading. The scatter of the experimental data was within 15%. An analysis of the experimental results allows us to draw the following conclusions: 1) with increasing distance s from the center of bending to the crack, the kink angle of the crack path α and the fracture load P also increase; 2) as each flank of the beam is additionally loaded by compressive stresses $\sigma = -1.25$ MPa, the fracture load P increases, and the kink angle of the crack path α substantially increases at $s > 20$ mm.

Using the experimental data obtained and the Russian Standard [9], we determine the critical stress-intensity factor (SIF) $K_{\mathrm{I}c}$ as

$$K_{\mathrm{I}c} = PY_1/(t\sqrt{b}\,) = 0.53 \text{ MPa} \cdot \text{m}^{1/2}, \tag{1}$$

where $Y_1 = 2.29$ is the correction function for $l/b = 0.45$. The critical SIF predicted by Eq. (1) differs from the SIF value given in the reference book [10], where $K_{\mathrm{I}c} \approx 1$ MPa $\cdot$ m$^{1/2}$.

2.2. *Experiments with Specimens Made of Fine-Grained Concrete.* Two types of neat cement (M 400 and Portland cement) were used to prepare fine-grained concrete specimens for strength studies aimed at constructing a strength curve of the Coulomb–Mohr type. The specimens were prepared from a mixture of sand and cement (2 : 1), and the size of sand particles was within 2 mm. The time of specimen solidification at a temperature of 20–22°C was 30 days. The tensile and compressive strengths were determined. In tensile tests, the specimens were shaped as a spade 40 mm long with a (20×51)-mm cross section in the middle part. In compressive tests, the specimens had the shape of a $(52 \times 52 \times 52)$-mm cube. In tensile tests, the specimens were subjected to elastic deformation up to their fracture (the modulus of elasticity under tension was $E = 400$ MPa). To obtain the limiting strength curve of the Coulomb–Mohr type, we performed experiments with specimens under shear loading with and

TABLE 2

Experimental Dependence $\sigma(\varepsilon)$ for the Plexiglas Specimen under Tension

$\sigma(\varepsilon)$, MPa	$\varepsilon \cdot 10^{-2}$	$\sigma(\varepsilon)$, MPa	$\varepsilon \cdot 10^{-2}$
0	0	40.0	1.76
10.0	0.40	43.2	2.08
20.0	0.82	45.4	2.28
25.0	1.04	48.0	2.55
30.0	1.24	48.1	2.80
35.0	1.42	47.9	3.00

TABLE 3

Experimental Dependence $\sigma(\tau)$ for the Plexiglas Specimen

σ, MPa	τ, MPa	σ, MPa	τ, MPa
48	0	−26	76
−124	0	−36	78
0	52	−57	81
−14	67		

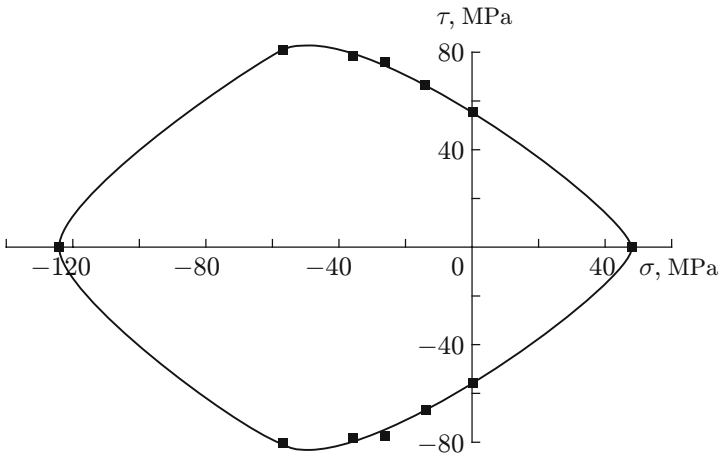

Fig. 5. Strength curve of the Coulomb–Mohr type for Plexiglas.

without preliminary compression. Specimens with a cross-sectional size of 25×25 mm and a length of 75 mm were tested under shear loading. The specimen, which was preliminary compressed over its length, was placed between two rigid piers located at a distance of 25 mm from each other. The shear load was applied to the (25×25)-mm cross section. The value of the compressive load was measured by a dynamometer. Three to five specimens were tested in each series of experiments. The maximum deviation of the experimental data from the mean values listed in Table 5 was within 14%.

Figure 6 shows the strength curves of the Coulomb–Mohr type in the plane (σ, τ), which describe the limiting stress states of fine-grained concrete for two types of cement.

For tests with three-point bending, the cracked fine-grained concrete beams were made on the basis of the Portland cement. In tests of the beams with a prescribed length of the edge crack l, we determined the kink angle of the crack path α as a function of the distance s from the center of specimen bending (the width of the cut simulating the crack was 1 mm). The specimen sizes were chosen to fit the Russian Standard (GOST) [9]: $L = 200$ mm, $b = 50$ mm, $l = 22.5$ mm, and $t = 25$ mm. The dependence of the kink angle α on the distance s was determined for two types of loading: $\sigma = 0$ and $\sigma \neq 0$ (see Fig. 1). Preliminary compression of the beam applied to the beam flanks corresponded to the value $\sigma = -1.25$ MPa. At least three tests were performed for each specimen. The results of these tests are summarized in Table 6.

The conclusions about the interrelations between the parameters s, α, and P, which were drawn from the analysis of the experimental results, are almost the same as those for the Plexiglas specimens.

The conducted experiments make it possible to determine the critical SIF in accordance with the Russian Standard [9]. This was performed in [11], where the experimental and calculated values of the critical SIF were found to be in reasonable agreement.

3. Discussion of Results. Let us analyze the results of the conducted experiments and compare them with the data from the reference books [7, 8]. The strength curves of the Coulomb–Mohr type in the plane (σ, τ) can be approximately described by using the points $(\sigma, \tau) = (\sigma_+, 0)$, $(\sigma, \tau) = (\sigma_-, 0)$, and $(\sigma, \tau) = (0, \pm\tau_0)$ on this

TABLE 4

Experimental Dependence
of the Kink Angle of the Crack Path α and the Fracture Load P
versus the Distance s between the Crack and the Center of Bending for the Plexiglas Specimens

s, mm	$\sigma = 0$		$\sigma = -1.25$ MPa	
	P, N	α, deg	P, N	α, deg
0	470	0	529	0
10	588	13	637	13
20	706	20	882	20
30	1039	25	1078	37
35	1509	40	—	—

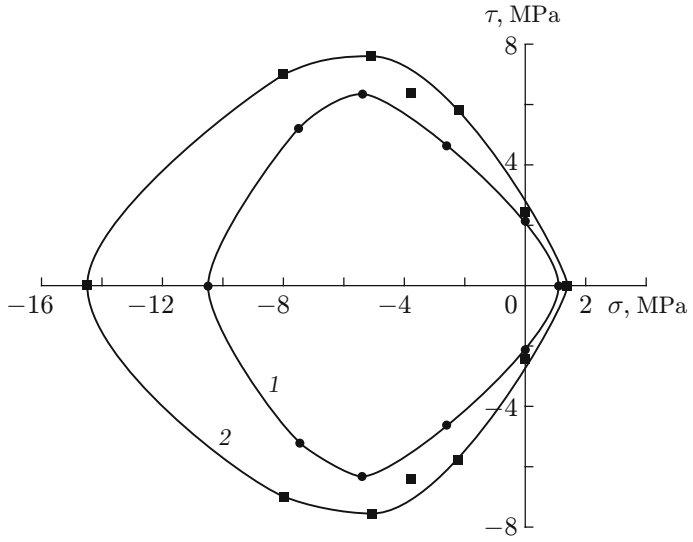

Fig. 6. Strength curves of the Coulomb–Mohr type for the fine-grained concrete specimens made with the use of M 400 cement (1) and Portland cement (2).

curve and the parameter tan γ (σ_+ and σ_- are the strength limits under tension and compression, respectively,τ_0 is the resistance to pure shear, and γ is the angle of "friction"; all these parameters were obtained in the absence of hydrostatic pressure). For the materials considered, we can form dimensionless constants τ_0/σ_+ and $|\sigma_-|/\sigma_+$. The first constant characterizes the brittleness (if $\tau_0/\sigma_+ \approx 1$) or viscosity (if $\tau_0/\sigma_+ \ll 1$) of the material under fracture. The second constant characterizes the resistance of the material to fracture under tension and compression. These constants allow the angles of crack branching and the kink angles of the crack paths to be determined [1, 2].

The dimensionless constants for Plexiglas, fine-grained concrete on the basis of the M 400 and Portland cement, and for a close-packed layer of atoms (the forces of atomic interaction were determined with the use of the Morse potential [12]) are listed in Table 7. The materials presented in Table 7 are characterized by brittle fracture, because $\tau_0/\sigma_+ \approx 1$ for Plexiglas and for a close-packed layer of atoms and $\tau_0/\sigma_+ > 1$ for fine-grained concrete. Note that only one value of the parameter tan γ is given in Table 7 for the case with $\sigma = 0$ (for $\sigma \neq 0$, this parameter becomes substantially different). The concrete specimens under study exhibit low resistance to tension. The reference books [7, 8] give the parameters of the fracture curves for the case of compression only, i.e., for the second and third quadrants in the plane (σ, τ). In contrast to the data in [7, 8], the present paper provides the limiting fracture curves in four quadrants on the plane (σ, τ), which is important for finding the angles of crack branching and kinking [1, 2]. The value of the parameter tan γ for fine-grained concrete is in good agreement with the value of the corresponding parameter for sandstone (see [7, Table 11-4]).

Conclusions. The limiting strength curves of the Coulomb–Mohr type were constructed on the basis of the results of experiments conducted with Plexiglas and fine-grained concrete specimens. Based on the dimensionless

TABLE 5

Experimental Dependence $\sigma(\tau)$ for the Fine-Grained Concrete Specimen

M 400 cement		Portland cement	
σ, MPa	τ, MPa	σ, MPa	τ, MPa
1.1	0	1.3	0
−10.7	0	−14.5	0
0	2.13	0	2.3
−2.6	4.60	−2.2	5.8
−5.4	6.30	−3.8	6.4
−7.5	5.20	−5.1	7.6
—	—	−8.0	7.0

TABLE 6

Experimental Dependence of the Kink Angle of the Crack Path α and the Fracture Load P versus the Distance s between the Crack and the Center of Bending for the Fine-Grained Concrete Specimens

s, mm	$\sigma = 0$		$\sigma = -1.25$ MPa	
	P, N	α, deg	P, N	α, deg
0	235	0	519	0
20	284	14	588	24
30	353	27	637	32
50	412	32	676	40
60	539	36	706	42

TABLE 7

Dimensionless Constants τ_0/σ_+, $|\sigma_-|/\sigma_+$, and $\tan\gamma$ for Various Materials

Material	τ_0/σ_+	$\lvert\sigma_-\rvert/\sigma_+$	$\tan\gamma$
Plexiglas	1.08	2.58	0.76
M 400 cement	1.94	9.70	1.12
Portland cement	1.77	11.20	1.26
Close-packed layer of atoms	1.02	0.82	1.03

parameters for these curves, it was found that the fracture of Plexiglas and fine-grained concrete can be classified as the quasi-brittle and brittle types, respectively. For fine-grained concrete, the value of the "friction" angle almost coincides with the value of the corresponding parameter for sandstone. The behavior of sandstone under fracture, therefore, can be modeled in the first approximation on the basis of results for fine-grained concrete. Processing of the experimentally obtained dependences of the kink angle of the crack paths on the stress state parameters in the case of three-point bending applied to Plexiglas and fine-grained concrete beams and comparisons with theoretical predictions were not performed, because the simple theory proposed in [1, 2] is valid only for mode I fracture.

This work was supported by the Russian Foundation for Basic Research (Grant No. 07-01-00163) and by the Integration Program of the Presidium of the Russian Academy of Sciences (Project No. 11.16).

REFERENCES

1. V. M. Kornev, "Fracture of brittle and viscous crystals. Force and strain criteria," *Prikl. Mat. Mekh.*, **67**, No. 6, 1029–1041 (2003).
2. V. M. Kornev, "Branching and kink of opening crack paths in polycrystals," *Fiz. Mezomekh.*, **6**, No. 5, 37–46 (2003).
3. J.-B. Leblond and J. Frelat, "Crack kinking from an initially closed crack," *Int. J. Solids Struct.*, **37**, 1595–1614 (2000).
4. K. G. Schmitt-Thomas, *Metallkunde für das Maschinenwesen*, Springer-Verlag (1989).

5. F. Erdogan and G. Sih, "On the crack extension in plates under plane loading and transverse shear," *Trans. ASME, Ser. D: J. Basic Eng.*, **85**, No. 4, 519–525 (1963).
6. S. Fliss, H. S. Bhat, R. Dmowska, and J. R. Rice, "Fault branching and rupture directivity," *J. Geophys. Res.*, **110**, B06312 (2005).
7. D. Hendin, *Strength and Plasticity: Reference Book for Rock Constants* [Russian translation], Mir, Moscow (1969).
8. *Catalogue of Mechanical Properties of Rocks* [in Russian] All-Union Research Mine Surveyor Institute, Leningrad (1972).
9. GOST 25.506-85, "Methods of mechanical testing of metals. Determining the characteristics of crack resistance under static loading," Valid since 03.27.85.
10. S. E. Kovchik and E. M. Morozov, *Mechanics of Fracture and Strength of Materials*, Vol. 3: *Characteristics of Crack Resistance of Materials and Methods of Their Determination* [in Russian], Naukova Dumka, Kiev (1988).
11. V. M. Kornev and A. G. Demeshkin, "Critical stress-intensity factor in the case of bending of concrete beams with a transverse crack," *Izv. Vyssh. Uchebn. Zaved., Stroitel'stvo*, No. 8, 10–19 (2007).
12. N. S. Astapov and V. M. Kornev, "Stability region of a close-packed layer of atoms," *J. Appl. Mech. Tech. Phys.*, **48**, No. 1, 135–144 (2007).